The Planetary Science Journal, 3:146 (13pp), 2022 June https://doi.org/10.3847/PSJ/ac7050

Variability in Titan's Mesospheric HCN and Temperature Structure as Observed by ALMA

Alexander E. Thelen[1,7], Conor A. Nixon[1], Richard G. Cosentino[2], Martin A. Cordiner[1,3], Nicholas A. Teanby[4], Claire E. Newman[5], Patrick G. J. Irwin[6], and Steven B. Charnley[1]

[1] Solar System Exploration Division, NASA Goddard Space Flight Center, Greenbelt, MD 20771, USA; alexander.e.thelen@nasa.gov
[2] Space Telescope Science Institute, Baltimore, MD 21218, USA
[3] Department of Physics, Catholic University of America, Washington, DC 20064, USA
[4] School of Earth Sciences, University of Bristol, Bristol BS8 1RJ, UK
[5] Aeolis Research, Chandler, AZ 85224, USA
[6] Atmospheric, Oceanic and Planetary Physics, Clarendon Laboratory, University of Oxford, Oxford OX1 3PU, UK

Received 2022 March 5; revised 2022 May 13; accepted 2022 May 13; published 2022 June 23

Abstract

The temperature structure of Titan's upper atmosphere exhibits large variability resulting from numerous spatially and temporally irregular external energy sources, seasonal changes, and the influence of molecular species produced via photochemistry. In particular, Titan's relatively abundant HCN is thought to provide substantial cooling to the upper atmosphere through rotational emission, balancing UV/EUV heating, and thermal conduction. Here we present the analysis of ALMA observations of Titan from 2012, 2014, 2015, and 2017, corresponding to planetocentric solar longitudes of ~34°–89°, including vertical HCN and temperature profiles retrieved from the lower mesosphere through the thermosphere (~350–1200 km; 3×10^{-2}–2×10^{-8} mbar). Throughout the atmosphere, temperature profiles differ by 10 to 30 K between observations approximately 1 Earth yr apart, particularly from 600 to 900 km. We find evidence for a large imbalance in Titan's upper atmospheric energy budget between 2014 and 2015, where the mesospheric thermal structure changes significantly and marks the transition between a mesopause located at ~600 km (2×10^{-4} mbar) and ~800 km (3×10^{-6} mbar). The retrieved HCN abundances vary dramatically during the 2012–2017 time period as well, showing close to 2 orders of magnitude difference in abundance at 1000 km. However, the change in HCN abundance does not appear to fully account for the variation in mesospheric temperatures over the $L_S \sim 34°–89°$ period. These measurements provide additional insight into the variability of Titan's mesospheric composition and thermal structure following its 2009 vernal equinox and motivate continued investigation of the origins of such rapid changes in Titan's atmosphere throughout its seasonal cycle.

Unified Astronomy Thesaurus concepts: Titan (2186); Natural satellite atmospheres (2214); Radiative transfer (1335); Submillimeter astronomy (1647); Planetary science (1255); Solar system astronomy (1529); Planetary atmospheres (1244); Remote sensing (2191); Astrochemistry (75)

1. Introduction

Titan, Saturn's largest moon, possesses a substantial atmosphere that is characterized by a thermal structure similar to that of the Earth, though colder and more vertically extended (up to ~1500 km), resulting from its comparatively reduced insolation and low gravity (see Flasar et al. 2014; Yelle et al. 2014; Hörst 2017, and references therein). Through observations by the Voyager 1 and 2 and Cassini spacecraft and direct measurements by the Huygens probe during its descent in 2005, Titan's atmospheric behavior and dynamics have been well studied through roughly half of its ~29.5 yr seasonal cycle (see, for example, Smith et al. 1982; Lindal et al. 1983; Vervack et al. 2004; Flasar et al. 2005; Fulchignoni et al. 2005; Shemansky et al. 2005; Yelle et al. 2006; Teanby et al. 2008, 2012; Snowden et al. 2013; Vinatier et al. 2015; Teanby et al. 2017, 2019; Sylvestre et al. 2020; Creecy et al. 2021; Seignovert et al. 2021; Sharkey et al. 2021). Additionally, measurements from ground-based observatories have helped to bridge gaps between missions to the Saturnian system (e.g., Kim et al. 2000; Geballe et al. 2003; Gurwell 2004; Moreno et al. 2005). However, the nature of short-term variability in the dynamical state of Titan's upper atmosphere, the seasonal evolution of its stratosphere (~80–300 km), and the contribution of many different chemical and dynamical components to Titan's atmospheric radiative budget still remain enigmatic after the end of the Cassini/Huygens mission.

Models of Titan's upper atmosphere—consisting of the mesosphere (typically defined as ~300–600 km), thermosphere (~600–1000 km), and ionosphere (>1000 km)—attempt to simulate Titan's atmospheric thermal structure through the balance of heating by solar EUV/UV photons, electron and ion precipitation, interactions with Saturn's magnetosphere and plasma sheet, thermal conduction, and cooling by rotational and vibrational emission from hydrogen cyanide (HCN) and various hydrocarbons produced via photochemistry (Yelle 1991; Müller-Wodarg et al. 2000, 2008; Yelle et al. 2008; Bell et al. 2010, 2011; Westlake et al. 2011; Bell et al. 2014; Snowden & Yelle 2014; Snowden & Higgins 2021). Additionally, atmospheric wave activity induced by gravitational tides may produce

---

[7] NASA Astrobiology Postdoctoral Program Fellow under the management of the Universities Space Research Association and Oak Ridge Associated Universities.

significant temperature perturbations in the upper atmosphere (Strobel 2006). These predictions, along with inferences of temperature from in situ density profiles obtained with the Cassini Ion and Neutral Mass Spectrometer (INMS) and Huygens Atmospheric Structure Instrument (HASI) and measurements derived through stellar occultations from the ground and the Cassini Ultraviolet Imaging Spectrograph (UVIS), revealed large variability in Titan's middle and upper atmospheric thermal structure on both diurnal and seasonal timescales. Further, observations from the Cassini Composite Infrared Spectrometer (CIRS), Imaging Science Subsystem (ISS), and Visible and Infrared Mapping Spectrometer (VIMS) instruments covering roughly half a Titan year indicated that Titan's radiative energy budget may not be fully balanced on both temporal (seasonal) and spatial (hemispheric) scales (Li 2015; Creecy et al. 2019, 2021), though further observations are required to determine the nature and effects of this imbalance on timescales of a Titan year or more.

Vertical perturbations of ∼10–30 K on ∼50–100 km scales (on order 1–2 scale heights) were present in the Huygens/HASI thermospheric measurements, indicating strong wave activity (Fulchignoni et al. 2005; Aboudan et al. 2008). Ionospheric measurements with the INMS revealed 30–60 K variations in temperature over a number of Cassini flybys between 2004 and 2010 and further evidence of wave activity on large (150–450 km) vertical scales (Müller-Wodarg et al. 2006; Snowden et al. 2013). These perturbations in temperature were found to be much larger in the upper atmosphere than in the lower mesosphere and stratosphere (Lorenz et al. 2014). Additionally, INMS measurements revealed warmer upper atmospheric temperatures on Titan's nightside and while it was within Saturn's plasma sheet; cooler temperatures were found on both the dayside and when Titan was in Saturn's magnetospheric lobe, though no strong correlation was found between temperature and latitude, longitude, solar zenith angle, or local solar time (Cui et al. 2009; Westlake et al. 2011; Snowden et al. 2013). UV occultations sounding Titan's middle atmosphere measured a mesopause at ∼650 km (Shemansky et al. 2005; Liang et al. 2007) and temperature inversions between 350 and 500 km attributed to Titan's seasonally variable detached haze layer (Sicardy et al. 2006; Lavvas et al. 2009), which was also detected with ISS and HASI (Porco et al. 2005; Fulchignoni et al. 2005; West et al. 2011).

As a strong contributor to both cooling Titan's upper atmosphere and producing further complex organic species, HCN provides substantial insight into Titan's innately linked chemical and dynamical systems. HCN was first detected on Titan by Voyager 1 (Hanel et al. 1981) and has been routinely observed in the millimeter regime (see, for example, Paubert et al. 1987; Hidayat et al. 1997; Marten et al. 2002; Courtin et al. 2011; Rengel et al. 2022). Following observations of CH_4 fluorescence in Titan's mesosphere—resulting in additional measurement of Titan's mesopause near 600 km (Kim et al. 2000)—HCN fluorescent emission was observed with the NIRSPEC instrument on Keck II by Geballe et al. (2003) and subsequently reanalyzed by Yelle & Griffith (2003) and Kim et al. (2005) to produce vertical profiles in Titan's mesosphere and thermosphere. These measurements and those from the Cassini VIMS, UVIS, and INMS instruments revealed Titan's HCN mole fraction to range between $\sim 3 \times 10^{-4}$ and 3×10^{-3} at 1000 km, along with evidence for diurnal variability (Shemansky et al. 2005; Magee et al. 2009; Koskinen et al. 2011; Adriani et al. 2011; Vinatier et al. 2015; Cui et al. 2016). In the stratosphere and mesosphere, the variability of Titan's HCN abundance has been studied using Cassini/CIRS, revealing dramatic enhancements at high latitudes larger than an order of magnitude throughout Titan's seasonal cycle (Teanby et al. 2007; Vinatier et al. 2015; Teanby et al. 2019). Further discrepancies exist between these observations and predictions from photochemical models (e.g., Loison et al. 2015; Willacy et al. 2016; Vuitton et al. 2019), raising additional questions pertaining to the role of HCN in Titan's chemical and radiative balance.

After the end of the Cassini/Huygens mission, ground-based observations continue to provide insight into Titan's complex atmospheric composition and dynamics on short-term and seasonal timescales. In particular, the Atacama Large Millimeter/submillimeter Array (ALMA) has proven to be a powerful facility to study planetary atmospheres and allows for the study of Titan's stratosphere through thermosphere by way of strong rotational emission lines from a variety of molecular species. Previous ALMA observations from 2012 to 2015 allowed for the study of temperature and HCN abundance in Titan's stratosphere during its northern spring (Molter et al. 2016; Serigano et al. 2016; Thelen et al. 2018, 2019a, 2019b), while spectral Doppler shift measurements revealed short-term variability in Titan's wind field in the middle and upper atmosphere (Lellouch et al. 2019, hereafter L19; Cordiner et al. 2020). Additionally, through the combination of carbon monoxide (CO) and HCN emission lines, L19 retrieved Titan's vertical temperature and HCN abundance profiles near the equator during 2016, showing a distinct mesopause at ∼800 km.

Here we analyze ALMA observations of Titan from 2012, 2014, 2015, and 2017 ($L_S \sim 34°$–$89°$) to determine the thermal structure and HCN abundance throughout Titan's upper atmosphere. These results are compared to previous measurements from the Cassini and Voyager missions, ground-based observations, and model predictions of Titan's atmosphere. We describe the observations and data reduction in Section 2 and the radiative transfer modeling process in Section 3. The results, comparisons to previous measurements and models, and discussion are presented in Section 4, followed by concluding remarks in Section 5.

2. Observations

Data from the ALMA main array, comprised of up to 50 12 m antenna dishes, were obtained from the ALMA Science Archive[8] covering the period 2012–2017. Observations of Titan were chosen such that the ALMA spatial resolution, often denoted by the FWHM of the point-spread function (PSF)—i.e., the synthesized beam—was $<0\farcs5$ (roughly half the angular size that Titan's solid body plus extended atmosphere subtends on the sky). The spectral resolution was high enough to resolve the ∼10 MHz wide HCN line core, enabling measurement of Titan's upper atmospheric temperature profile (L19). The same rotational transition of HCN was measured across multiple observations so as to directly compare the derived vertical HCN and temperature profiles; in this case, the HCN $J = 4-3$ transition at 354.505 GHz was used. The resulting parameters for selected archival observations with the qualities specified above are presented in Table 1, including a mix of dedicated Titan observations from 2012, 2016, and

---

[8] https://almascience.nrao.edu/aq/

Table 1
ALMA Observational Parameters

Project Code	Obs. Date	Int. Time (s)	Spec. Res. (kHz)	Chan. Width (kHz)	Spatial Res.[a] (arcsec)	Pos. Ang. (deg)	Subsol. Lat. (deg)	L_S[b] (deg)
2011.0.00727.S	2012 Jun 15	1572.6	122	61	0.470 × 0.365	52.60	12.64	34.34
2012.1.00635.S	2014 Apr 25	312.5	976	488	0.457 × 0.380	−81.53	22.10	55.68
2013.1.00446.S	2015 Jun 12	151.3	282	244	0.361 × 0.304	−67.06	24.28	68.41
2015.1.01023.S[c]	2016 Aug 19	2925.9	1938[d]	1953	0.265 × 0.144	52.13	26.07	81.59
2016.A.00014.S	2017 May 8	1080.0	976[d]	488	0.231 × 0.185	−75.85	26.41	89.49

Notes.
[a] Spatial resolution corresponds to the FWHM of the ALMA PSF.
[b] Refers to the solar longitude (measured from the vernal equinox) of Saturn.
[c] Previously analyzed by L19, shown here for reference.
[d] Higher spectral resolution windows centered just on the HCN line core were also included in these observations for the measurement of winds.

2017 and short observations from 2014 and 2015, where Titan was used as a flux calibration source. As the 2016 data were previously analyzed by L19, the observational parameters and spectra are only shown here for context and comparison.

The ALMA observations were reduced and calibrated in the Common Astronomy Software Application (CASA) package (Jaeger 2008) using the Joint ALMA Observatory (JAO) pipeline scripts provided with each observation. Typical pipeline calibration procedures included the correction of complex visibility gain and phase measurements and amplitude calibration using strong (sub)millimeter continuum sources, such as quasars or solar system moons (including Titan itself). For observations from 2014 and 2015, where Titan was used as a flux calibration target, the JAO scripts were modified to remove commands flagging spectral windows containing HCN emission lines, which are often removed during calibration procedures due to their strong, broad line wings. Calibrated visibilities were corrected to Titan's rest velocity frame using ephemeris data from the JPL Horizons System[9] and deconvolved to remove interferometric artifacts using the CASA `tclean` task. During imaging, pixel sizes were set to one-fourth to one-fifth of the ALMA synthesized beam size. The Högbom clean algorithm (Högbom 1974) was used, and additional weighting to long antenna baselines was applied using the Briggs weighting scheme with a robust parameter of 0.5 (Briggs 1995). The data were cleaned to a flux threshold of twice the rms noise.

Individual spectra were extracted from pixels at Titan's nadir and western limb and converted to radiance units for use during radiative transfer modeling using the procedures described in Thelen et al. (2018, 2019b). The nadir spectra of Titan's strong, rotational HCN emission lines are particularly sensitive to the mesospheric temperature structure (L19); comparisons of HCN nadir spectra are shown in Figure 1, with the inset showing differences in the line core depth between each observation. Simultaneously modeling both limb and nadir spectra allows for the retrieval of Titan's vertical thermal profile while mitigating degeneracy imposed by variability in the vertical HCN volume mixing ratio (VMR) profile (L19). To ensure that the HCN line core was fixed at the rest frequency, small spectral line shifts were added to the extracted limb spectra (on the order of 1–2× the ALMA channel spacing; Table 1) to account for Doppler shifts induced by upper atmospheric winds found in high-resolution observations of various molecular species (L19; Cordiner et al. 2020).

3. Radiative Transfer Modeling

As rotational HCN emission lines are pressure-broadened by Titan's atmosphere and thus vary in line shape due to changes in the atmospheric state with altitude (and as a result of the ALMA beam size and latitude), radiative transfer models were calculated independently for spectra from each observation to determine both the continuous vertical HCN VMR and temperature profiles from the top of the stratopause to the lower thermosphere. Modeling was performed using the Nonlinear optimal Estimator for MultivariatE spectral analySIS (NEMESIS) radiative transfer code developed by Irwin et al. (2008). Synthetic HCN spectra were calculated implicitly using NEMESIS in line-by-line mode using spectral line and partition function data from the Cologne Database for Molecular Spectroscopy[10] (Müller et al. 2001) and HITRAN catalog[11] (Gordon et al. 2022). Line broadening and temperature-dependence coefficients, collisionally induced absorption pairs, and initial gas profiles for N_2, CH_4, and H_2 were taken from Serigano et al. (2016), Molter et al. (2016), Thelen et al. (2018), and references therein. A priori vertical profiles for CO, HCN, and HC_3N were used from ALMA observations of Titan in 2012, 2014, and 2015 presented in previous analyses (Molter et al. 2016; Serigano et al. 2016; Thelen et al. 2018, 2019a, 2019b). The temperature and HCN a priori vertical profiles used here are shown in Figure 2.

Models of Titan's (sub)millimeter thermal emission were initialized using temperature profiles from Cassini Radio Science observations sensitive to Titan's troposphere and stratosphere at altitudes <100 km (Schinder et al. 2012, 2020). Spectral windows adjacent to the HCN $J = 4-3$ emission line were then used to determine offsets between the data and model continuum to derive a multiplicative corrective scaling factor (if needed), as described in Thelen et al. (2018); these corrective factors were on order 0.90–1.10, a typical uncertainty for flux density calibrations of ALMA with quasars and solar system objects (Fomalont et al. 2014).

As previous studies retrieved Titan's vertical temperature (using CO) and HCN profiles throughout Titan's stratosphere

---

[9] https://ssd.jpl.nasa.gov/horizons/app.html#/

[10] https://cdms.astro.uni-koeln.de

[11] https://hitran.org

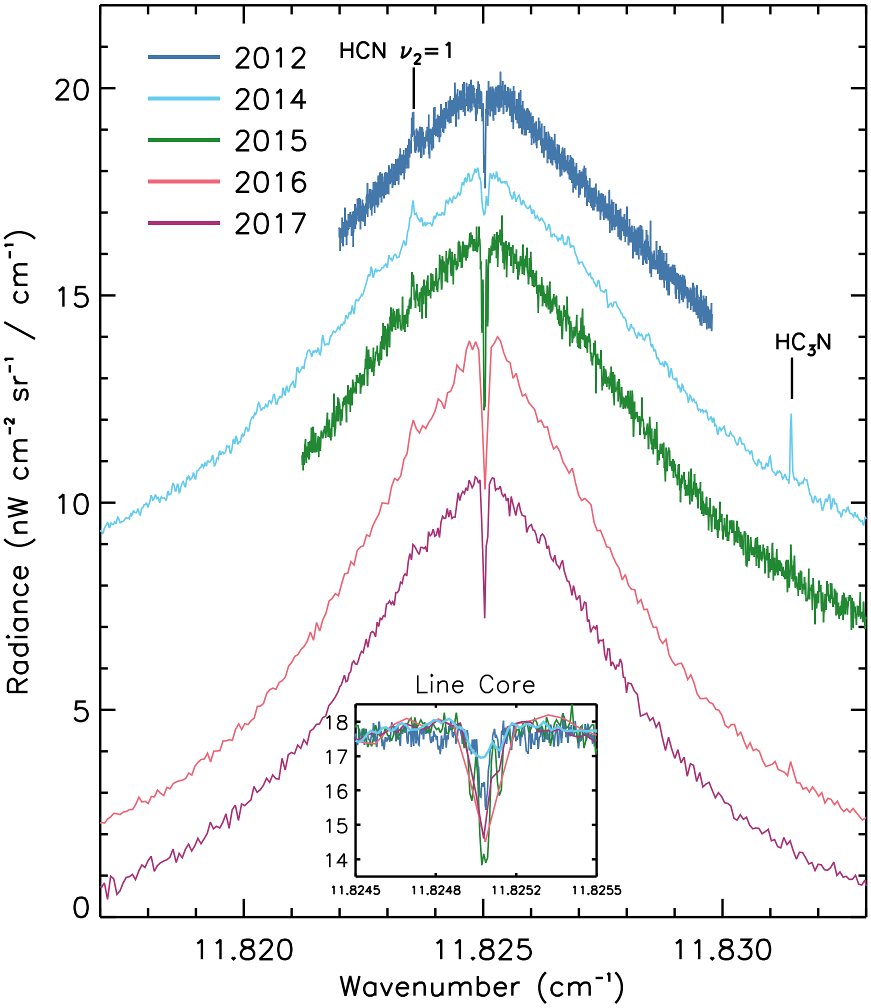

Figure 1. Titan HCN ($J = 4–3$) nadir spectra from ALMA observations in 2012 (blue), 2014 (cyan), 2015 (green), 2016 (red), and 2017 (purple). Spectra are vertically offset above or below the 2014 spectrum by subsequent multiples of 2 nW cm^{-2} sr^{-1}/cm^{-1} for clarity and plotted in radiance units to account for the change in beam size between observations. The inset shows comparisons of absorption in the HCN line core, which sounds Titan's mesopause, and the spectra have been shifted to compare absorption depths.

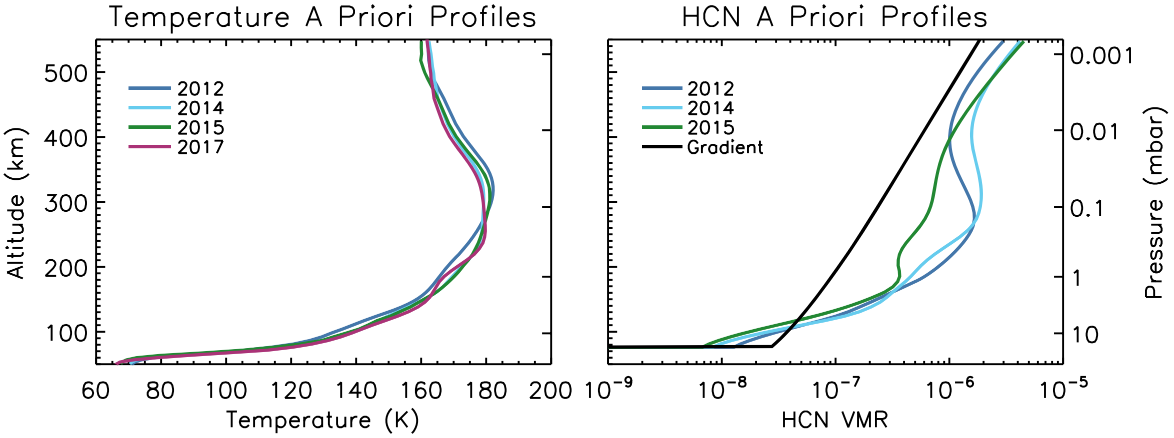

Figure 2. A priori vertical profiles used for radiative transfer modeling. (Left) Temperature a priori profiles from Thelen et al. (2018, 2019a) retrieved from ALMA CO spectra (100–550 km) and Cassini Radio Science data (<100 km) in 2012 (blue), 2014 (cyan), 2015 (green), and 2017 (purple). (Right) HCN VMR profiles retrieved from ALMA H^{13}CN and HC^{15}N spectra in 2012, 2014, and 2015 from Thelen et al. (2019b). A simple vertical gradient (black) was used to test the sensitivity of retrievals to vertical structure.

(Serigano et al. 2016; Molter et al. 2016; Thelen et al. 2018, 2019b), we parameterized NEMESIS models of HCN spectra such that the vertical temperature and HCN abundance were allowed to vary continuously above the stratopause (~250–350 km) in a grid of 108 atmospheric layers. Layers were separated vertically by 3–40 km, increasing with altitude.

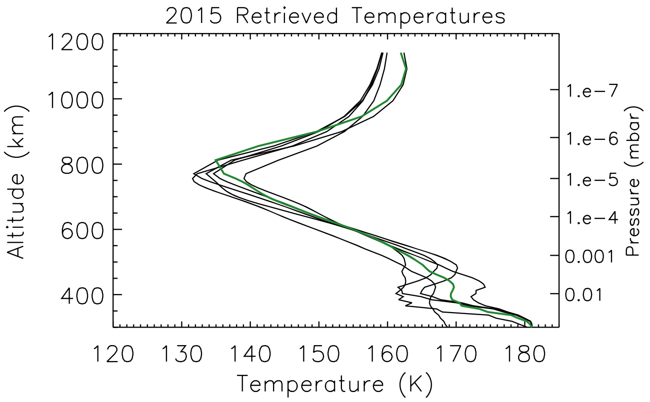

Figure 3. Comparison of retrieved temperature profiles from 2015 after using perturbations of the a priori temperature and HCN profiles shown in Figure 2 to illustrate the stability of the retrieved mesopause and lower mesospheric inversion near 400 km (∼0.01 mbar). The best-fit vertical profile is shown in green.

Simple a priori vertical profiles above the stratosphere were used to avoid imparting artificial vertical structure on the retrieved profiles. These include an isothermal profile at 160 K at altitudes >600 km and a simple vertical HCN gradient in log (VMR) from its condensation altitude at ∼80 km (Marten et al. 2002) up to a VMR $= 2 \times 10^{-4}$ at 1100 km (Vuitton et al. 2007). Subsequent model runs incorporated perturbations to the HCN profile by an order of magnitude in either direction or used the photochemical model profile of Loison et al. (2015) to test the sensitivity of the retrievals to vertical structure (Molter et al. 2016; L19). Unique vertical features, such as a small temperature inversion around 400 km (Figure 3), were considered valid if they manifested in the majority of retrievals. The correlation length for temperature and HCN profiles was set to 1.5 and 3.0 scale heights, respectively, so as to prevent unphysical vertical oscillations in the retrieved HCN profiles (Molter et al. 2016; Thelen et al. 2018). The 1σ errors on the vertical thermal profile were initialized at 1 K above the stratopause and raised to 5–10 K in the upper atmosphere, while the HCN a priori errors were set at 100% of the HCN VMR.

As in L19, the HCN abundance and temperature were retrieved simultaneously by fitting both nadir and limb spectra at once. While previous observations have shown Titan's thermospheric temperature and HCN abundance to vary with longitude (Snowden et al. 2013; Cui et al. 2016), we found the retrieved profiles from the east and west limbs to fall within the corresponding retrieval errors. To accurately model emission from the ALMA beam shape, 20 emission angles were used for each viewing geometry, as described in Thelen et al. (2018).[12] A representative set of emission angle weights are shown in Figure 4 for the observation from 2017 May 8 (ALMA Project Code 2016.A.00014.S). A smaller range of data points was modeled near the HCN line center at the native ALMA spectral resolution, allowing for higher weighting of the line core during the χ^2 minimization of iterative spectral inversions, thereby optimizing the sensitivity of the retrievals to the relevant atmospheric pressures. Derivatives calculated for the HCN $J = 4-3$ limb and nadir spectral radiances as a function of both HCN VMR and temperature are shown in Figure 5 (see Section 2.1 of Irwin et al. 2008 for a complete description of functional derivatives in the NEMESIS code). These functional derivatives illustrate the sensitivity of the HCN line core to Titan's temperature profile up to ∼1000 km and the complementary nature of limb and nadir spectral sensitivity to HCN abundance that helps to break the degeneracy in HCN and temperature retrievals (L19). The resulting best-fit limb and nadir spectra are shown in Figure 6; see the Supplementary Materials of L19 for the analysis of data from 2016.

4. Results and Discussion

The retrieved vertical profiles corresponding to the best-fit spectral models presented in Figure 6 are shown in Figures 7 and 8, accompanied by the retrieved temperature and HCN profiles from 2016 adapted from L19. As with previous observations of Titan's mesosphere and thermosphere, substantial variability is present between the four profiles derived here and that of L19 above ∼400 km (0.01 mbar), reaching maximum differences of 10–30 K. The differences across our retrieved temperatures are much larger than those found for the stratosphere during the same period with similar ALMA observations (generally ∼5 K from Earth year to year; Figure 2, left; Thelen et al. 2018). A distinct mesopause was found for all four observations analyzed here and in the profile derived from 2016 data by L19, as indicated by the presence of absorption in the HCN line core (Figure 1, inset) that is distinctly sensitive to the pressure, temperature, and HCN abundance of the atmosphere >600 km (Figure 5). The location and temperature of these relative minima are largely different from one observation to the next. This is also clearly visible in the raw spectra as differences in the relative depth and shape of the HCN line cores. The warmest and lowest temperature minimum, 153.7 ± 4.0 K at 563 ± 10 km (∼3.8×10^{-4} mbar), was found in 2014 ($L_S \sim 56°$). The coldest and highest mesopause, 134.9 ± 3.4 K at 812 ± 42 km (∼3.3×10^{-6} mbar), was found in 2015 ($L_S \sim 68°$), just under 26 Titan days (413 Earth days) later. The 2012 and 2017 measurements and those found by L19 are bracketed by these extremes, resulting in a distinct and rapid separation between the 2012 and 2014 ($L_S \sim 34°$–$56°$) observations and those after 2015 ($L_S \geqslant 68°$). The upper atmospheric temperatures vary between 153 K (2016; L19) and 165 ± 4.4 K (2014) at 1200 km (2.0×10^{-8} mbar), while the largest temperature difference in the lower mesosphere is found at ∼450 km (4.6×10^{-4} mbar) between 2015 and 2016, where the temperature varies between 155 ± 3.8 and 169 ± 3.0 K. Authors L19 noted a stable, quasi-isothermal region in their retrieved profiles from ∼450–600 km, which was also evident in the a priori profiles they employed based on data from Cassini/CIRS. Similarly, a small temperature inversion was found to be stable in our 2012, 2015, and 2017 results, as shown in the inset in Figure 7. These inversions may be attributed to Titan's detached or transient haze layers, as discussed further in Section 4.2.2.

The retrieved vertical HCN profiles, as shown in Figure 8, show similarly large variability between the four observations analyzed here. In particular, the 2012 spectrum required substantially lower HCN abundance throughout the atmosphere above ∼600 km (2.5×10^{-4} mbar), resulting in an order of magnitude less HCN in the lower atmosphere than the other retrievals and ∼30× less than the 2014 and 2016 (L19) profiles near 1100 km (7.6×10^{-8} mbar). Attempts to fit the spectrum from 2012 using the retrieved HCN profiles from 2014 a priori

---

[12] The ALMA spectrum extraction and emission angle weighting code may be found at https://data.mendeley.com/datasets/szbcb44s43/1 (Thelen & Molter 2018).

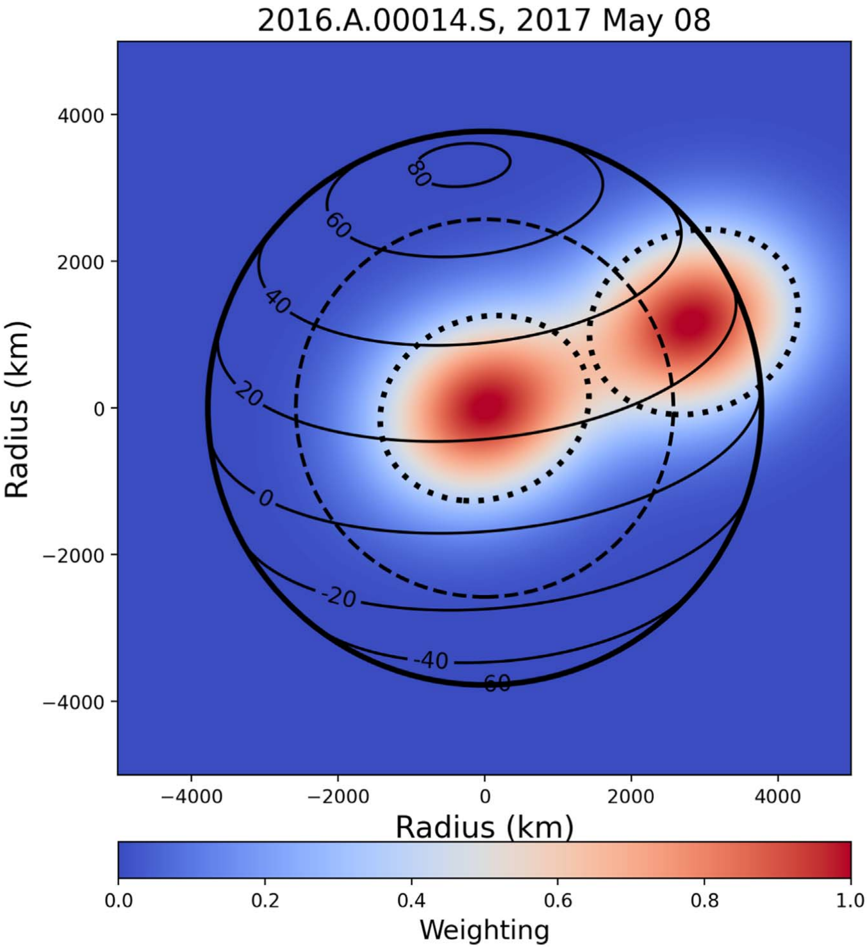

Figure 4. Weighting function distribution for nadir and limb viewing geometries for the 2017 observation. Beam locations were placed such that the top-of-atmosphere latitudes matched for both locations for each observation, taking into account Titan's tilt. Weighting distributions are not coadded, as plotted, but calculated individually for each extraction region. Titan's solid body radius (2575 km; dashed circle), top of atmosphere (1200 km above the surface; solid circle), and top-of-atmosphere latitudes are shown. The FWHM of the ALMA beam is denoted by the dashed ellipses.

resulted in large reduced χ^2 values for spectral fits and required significant or physically unlikely deviations from the input profiles. This suggests that the atmosphere in Titan's low northern latitudes during 2012 was depleted of HCN above the mesopause (occurring near this location in 2012) by a factor of 2–30. Similarly, the 2015 and 2017 retrievals require roughly an order of magnitude less HCN above ~800 km (7.4×10^{-6} mbar) than those of 2014 and 2016 (L19). The retrieved HCN VMR values at 1000 km, along with the mesopause altitudes and temperatures, are plotted as a function of time in Figure 9. While the distinct transition between the 2014 and 2015 mesopause locations and magnitudes is evident here, a correlation with the HCN abundance is not apparent.

4.1. Comparisons to Previous Studies

Our results are compared to previous measurements and predictions of Titan's thermal profile in Figure 10. Titan's mesospheric temperature profiles appear to transition between two states, with a mesopause at ~600 or 800 km, similar to previous measurements by Kim et al. (2000) and Liang et al. (2007; revised from Shemansky et al. 2005) in 1999 and 2004, respectively. Our profiles also agree with the altitudes of the mesopause predicted by the atmospheric models of Lellouch et al. (1990) and Yelle et al. (1997), though the magnitude of the mesopause temperature is only matched by the Lellouch et al. (1990) model in 2015; our 2014 profile is significantly warmer (~20 K) than the results of Yelle et al. (1997), despite the similar location of the inversion. These comparisons may reflect the differences in the incorporated physics and inclusion of HCN cooling between the two models (Yelle 1991), while the discrepancy with the model of Yelle et al. (1997) may be due to assumptions of or seasonal variations in aerosol heating and CH_4 or C_2H_6 abundances, which affect the temperature profile more strongly at ~600 km (Yelle 1991). Our retrieved mesopause temperatures are generally warmer than previous observations from earlier in Titan's seasonal cycle, though they occur at similar altitudes, with the exception of the profile derived from HASI measurements during the Huygens descent, where a temperature minimum of 152 K was found at ~490 km. We find warmer upper atmospheric temperatures than the average profile measured by Cassini/INMS, though within one standard deviation (125–165 K at 1200 km) observed over a large number of flybys (Snowden et al. 2013). The retrieved profiles are generally cooler than the models of Bell et al. (2010, 2014) and do not exhibit a mesopause at ~900 km, as seen there; however, the temperatures above those altitudes are generally in good agreement. Our retrieved temperature profiles tend to relax toward the a priori value of 160 K above ~1100 km, where the spectra are less sensitive to deviations in the temperature profile (Figure 5), consistent with the thermospheric model of Müller-Wodarg et al. (2008) at 1000 km for low

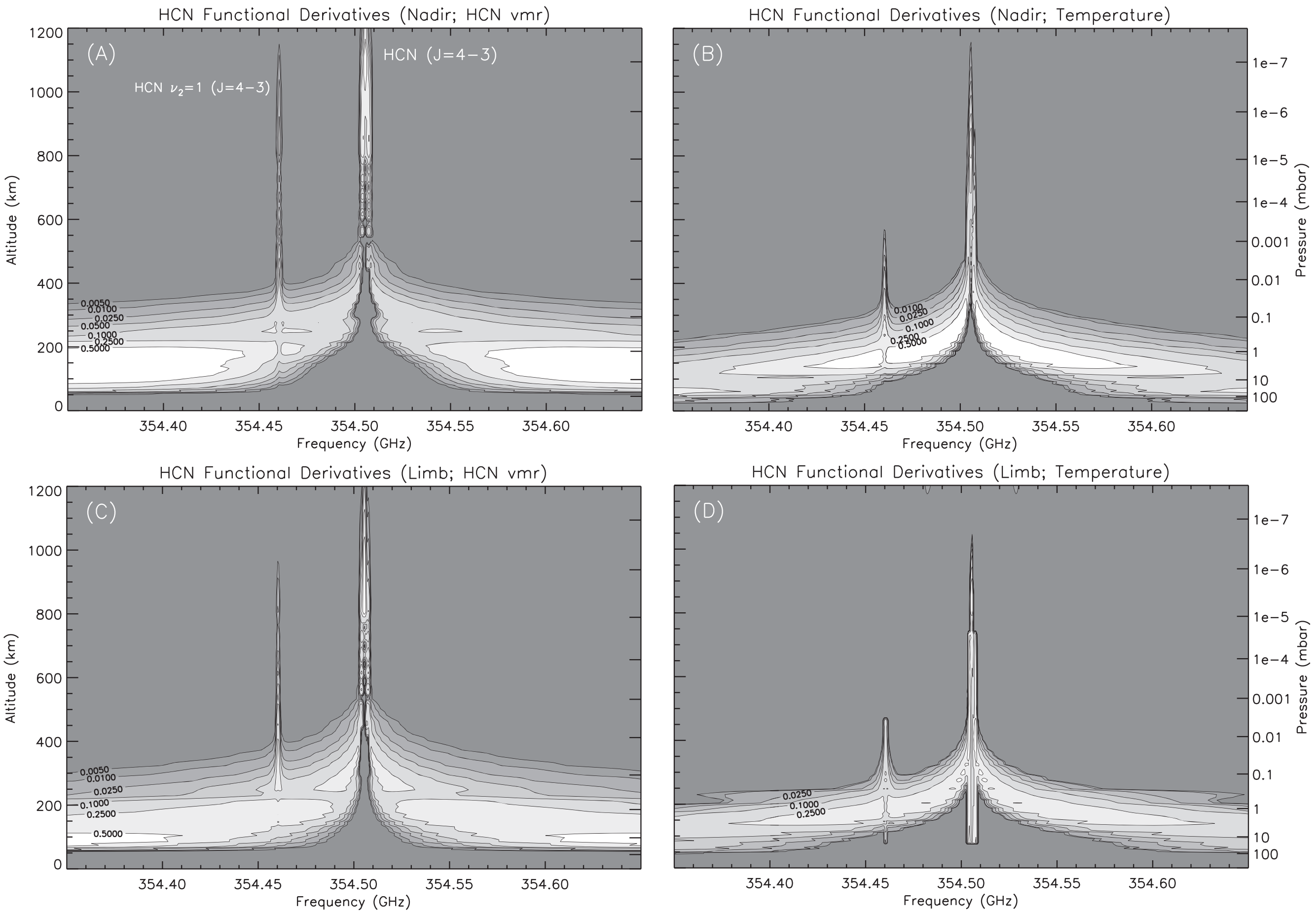

Figure 5. Plots of normalized functional derivatives calculated by NEMESIS for HCN ($J = 4-3$) spectra as a function of frequency and altitude with respect to HCN VMR (left column) and temperature (right column) in nadir and limb viewing geometries (top and bottom row, respectively). Contours increase with relative contribution.

northern latitudes (164 ± 6 K at 20° N). The profiles derived from ALMA observations between 2012 and 2017 are consistent with the range of values found through contemporaneous observations with the Cassini/CIRS instrument in the lower mesosphere (see Mathé et al. 2020, as depicted by the range of temperatures in orange in Figure 10, and Vinatier et al. 2020). Compared with the stratosphere, which varies significantly at high latitudes and on seasonal timescales (Sylvestre et al. 2020; Sharkey et al. 2021), the derived mesospheric temperature profiles from ALMA observations present evidence for larger-magnitude thermal variability within low-latitude regions on shorter timescales.

Previous measurements of Titan's upper atmospheric HCN by ground-based observations and Cassini are compared to our retrieved 2014 and 2015 ($L_S \sim 56°$ and 68°) profiles in Figure 11. Results from Cassini UVIS and VIMS observations (Shemansky et al. 2005; Koskinen et al. 2011; Adriani et al. 2011) and the NIRSPEC instrument on Keck II (Yelle & Griffith 2003; Kim et al. 2005) show generally higher HCN abundances in the upper atmosphere than found with the Cassini INMS instrument (Magee et al. 2009; Cui et al. 2016) and predicted by photochemical models (Willacy et al. 2016; Vuitton et al. 2019; Dobrijevic et al. 2021). While our 2014 ($L_S \sim 56°$) retrieval and that of L19 in 2016 ($L_S \sim 82°$) fall somewhere in the middle of these prior observations, the 2012, 2015, and 2017 results deviate further still above ~900 km, extending the range of measured HCN in Titan's upper atmosphere from $\sim 3 \times 10^{-5}$ to 3×10^{-3}, with relative maxima occurring at altitudes of ~950–1100 km. While atmospheric nitriles (e.g., HC_3N) have been found to vary with latitude up to 2 orders of magnitude between Titan's equator and winter pole in the stratosphere (Teanby et al. 2007; Vinatier et al. 2015), we find that the temporal HCN variability is far more significant in the upper atmosphere throughout its year compared to contemporaneous retrievals in the stratosphere at low latitudes by the Cassini CIRS instrument (Teanby et al. 2019; Coustenis et al. 2020; Mathé et al. 2020; Vinatier et al. 2020).

4.2. Interpretations

4.2.1. Upper Atmospheric Energetics and Dynamics

Compared to Titan's stratosphere, which evolves on seasonal timescales (Flasar et al. 1981), the upper mesosphere and thermosphere exhibit short-term variability due to the complex, highly variable environment Titan encounters during its passage through Saturn's nonuniform magnetosphere and gravitational potential (due to Titan's orbital eccentricity ~0.03) and its changing insolation. Above 1000 km, we measure variations of 3–10 K between observations, likely resulting from the combined effects of environmental factors such as changes in charged particle precipitation (found to increase the temperature by ~7 K by Snowden & Yelle 2014) and Titan local time (de La Haye et al. 2008). These changes typically affect Titan's thermosphere on much shorter

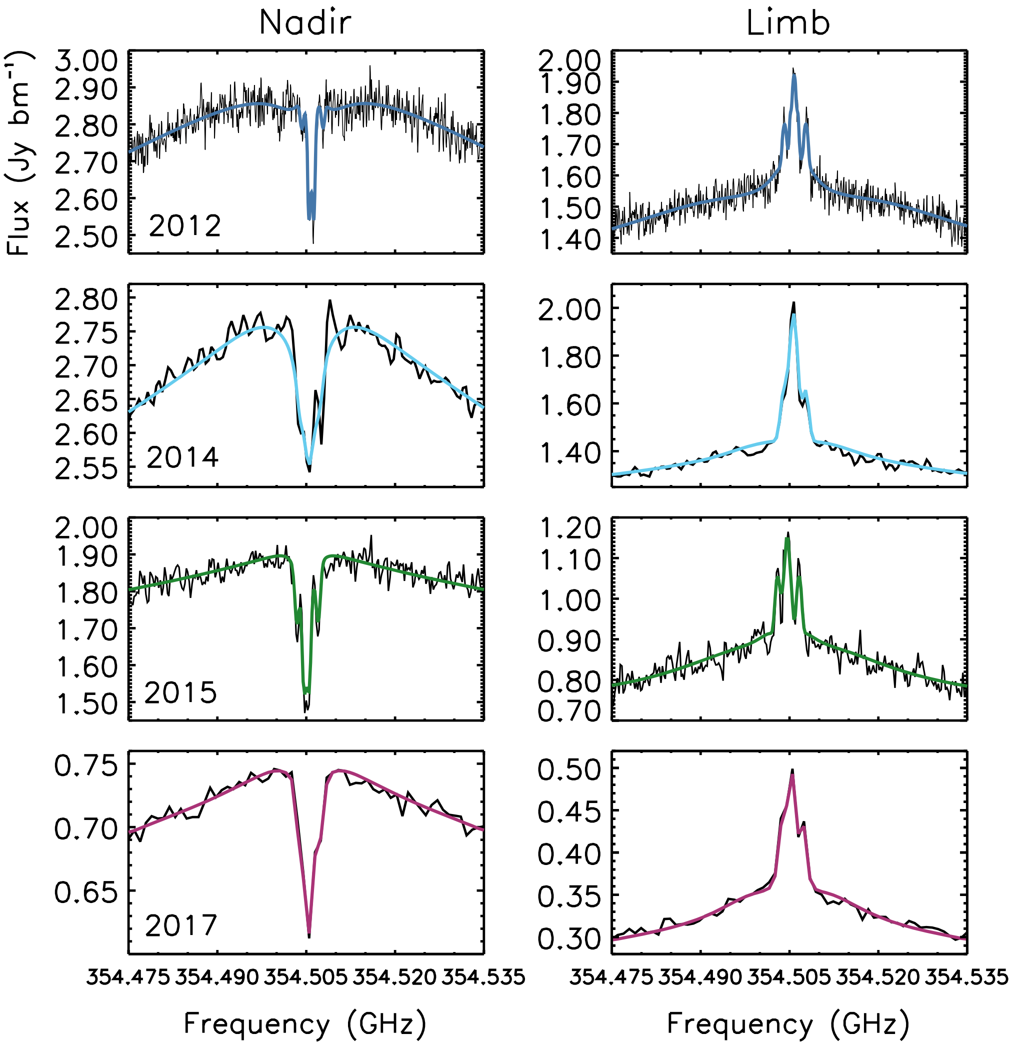

Figure 6. ALMA spectra (black) extracted from nadir (left column) and limb (right column) pixels compared with the best-fit NEMESIS models (colored lines) for 2012 (first row), 2014 (second row), 2015 (third row), and 2017 (fourth row).

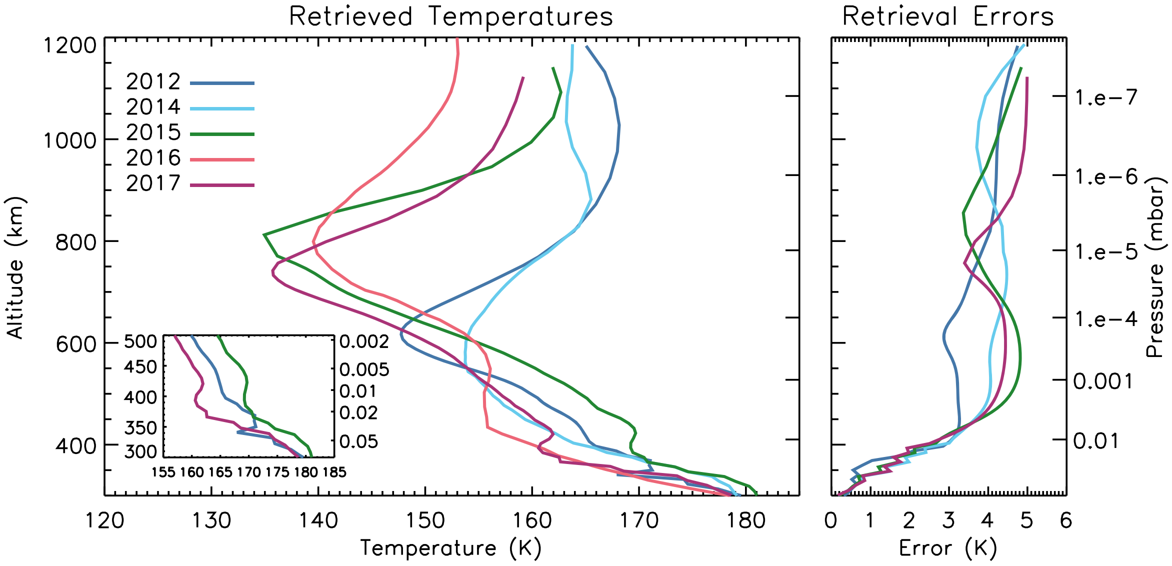

Figure 7. (Left) Retrieved vertical temperature profiles corresponding to the NEMESIS best-fit models in Figure 6. The retrieved temperature profile from L19 is shown in red for comparison. (Inset) Comparison of the retrieved 2012, 2015, and 2017 profiles near the location of Titan’s detached haze layer. (Right) Errors on the retrieved 2012, 2014, 2015, and 2017 models. The pressure scale on the right *y*-axis is approximate.

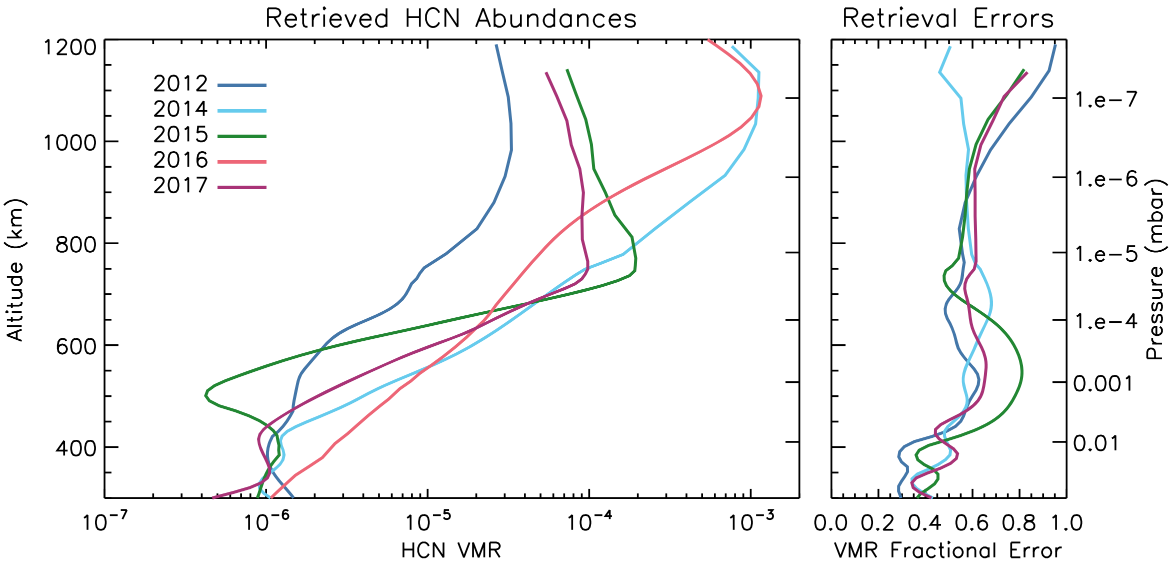

Figure 8. (Left) Vertical HCN VMR profiles corresponding to the NEMESIS best-fit models in Figure 6, retrieved simultaneously with the temperature profiles in Figure 7. The retrieved HCN profile from L19 is shown in red for comparison. (Right) Fractional errors on the retrieved 2012, 2014, 2015, and 2017 VMR profiles. The pressure scale on the right *y*-axis is approximate.

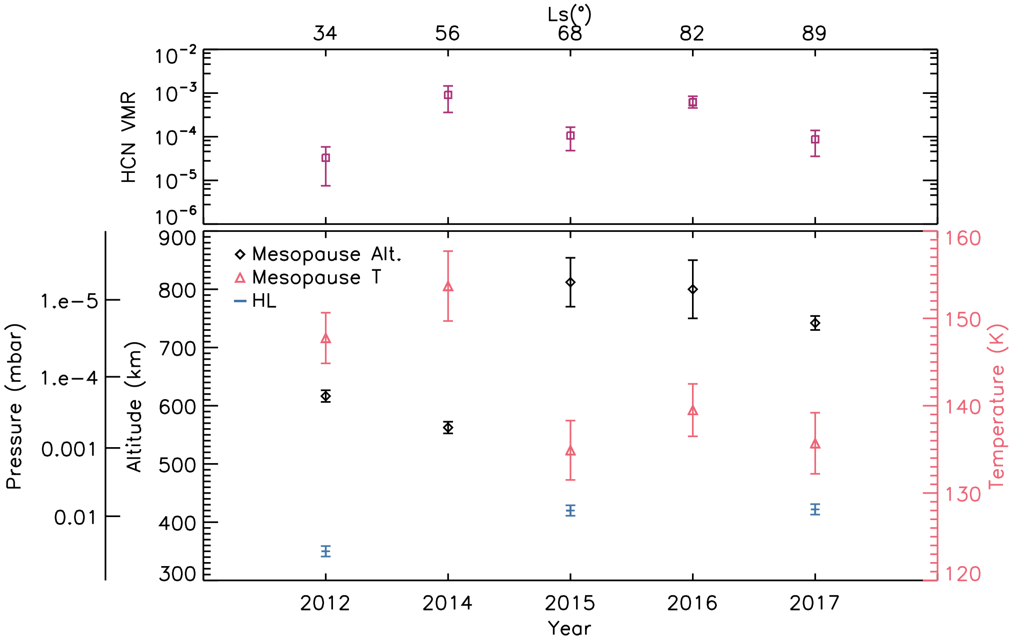

Figure 9. (Top) HCN VMR at 1000 km as a function of time. (Bottom) Mesopause (black diamonds) and haze layer (blue lines) altitudes (left *y*-axis) and mesopause temperatures (red triangles; right *y*-axis) as a function of time. The secondary pressure axis is approximate.

timescales than the time between observations analyzed here (on the order of 1 Titan day; Bell et al. 2011; Snowden & Yelle 2014), so while the effects of energy sources from the external environment are present, they are difficult to quantify directly and compare from one observation to the next.

No clear trend between the measured temperatures and Titan's orbital position with respect to the Saturnian magnetosphere is apparent across the small sample size of data analyzed here. Titan's location during the 2014 and 2016 observations is very similar—to the west of Saturn, in the ram direction with respect to the Saturnian magnetosphere (see descriptions in Rymer et al. 2009 and Westlake et al. 2011)—though the thermal structure varies dramatically between these two dates. Titan was observed completely outside of Saturn's magnetosphere by Cassini during 2013 December, roughly 8 Titan days before the 2014 ALMA observation (Bertucci et al. 2015). The effects of the 2013 event, during which Titan was directly exposed to solar wind particles, may be indirectly seen in the difference in the temperature and HCN profiles between the 2012 and 2014 observations. Similarly, this time period also marked the maximum of solar cycle 24, which may increase the EUV flux experienced by Titan compared to many of the Cassini observations made during solar minimum (Yelle et al. 2014).

The effects of HCN cooling are significant at altitudes >700 km, as a variation in HCN abundance by ∼an order of magnitude may cool the atmosphere by ∼20 K (Yelle 1991; Bell et al. 2010; Snowden & Yelle 2014). This may help explain the warmest thermospheric temperatures in the 2012

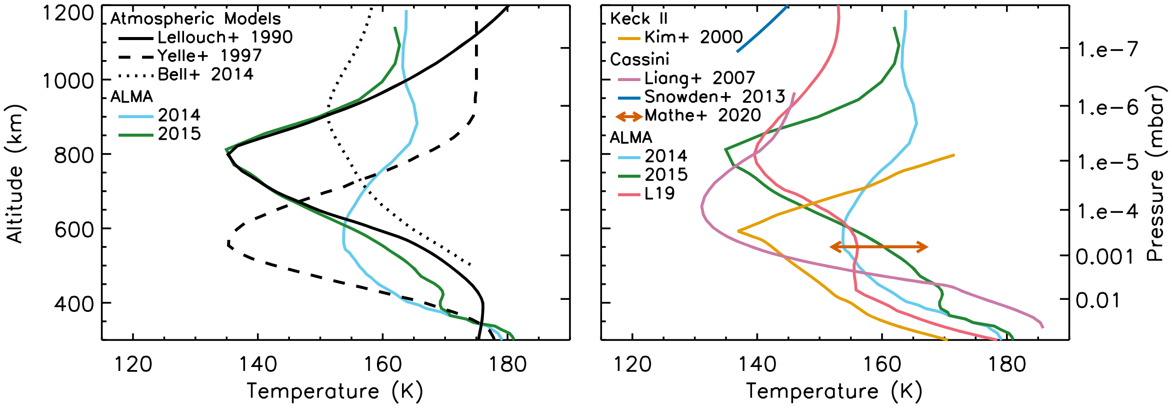

Figure 10. Comparison of the retrieved 2014 ($L_S \sim 56°$; cyan) and 2015 ($L_S \sim 68°$; green) temperature profiles to (left) atmospheric model predictions from Lellouch et al. (1990), Yelle et al. (1997), and Bell et al. (2014; their model C) and (right) ground-based observations (Kim et al. 2000; L19) and measurements from the Cassini UVIS (Liang et al. 2007), INMS (Snowden et al. 2013), and CIRS (Mathé et al. 2020, shown as a range of equatorial temperatures measured from 2010 to 2017) instruments. The pressure scale on the right *y*-axis is approximate.

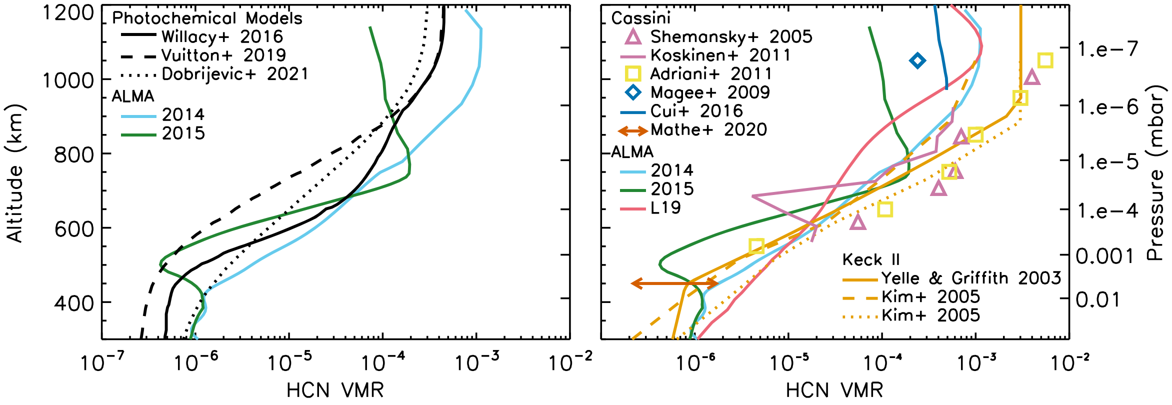

Figure 11. Comparison of the retrieved 2014 ($L_S \sim 56°$; cyan) and 2015 ($L_S \sim 68°$; green) HCN vertical profiles to (left) photochemical model results (Willacy et al. 2016; Vuitton et al. 2019; Dobrijevic et al. 2021) and (right) ground-based observations (Yelle & Griffith 2003; Kim et al. 2005; L19) and Cassini UVIS (Shemansky et al. 2005; Koskinen et al. 2011), VIMS (Adriani et al. 2011), INMS (Magee et al. 2009; Cui et al. 2016), and CIRS (Mathé et al. 2020, as in Figure 10) measurements. The pressure scale on the right *y*-axis is approximate.

($L_S \sim 34°$) profile, where HCN abundances were found to be significantly less than the other three observations and the measurements of L19 ($L_S \sim 82°$). The thermal profile of L19 is cooler than the profiles we retrieved above ~950 km and accompanied by a relatively high HCN abundance in the thermosphere, while our profiles from 2015 and 2017 are warmer and require less HCN. The temperature and HCN profiles from 2014 ($L_S \sim 56°$) remain puzzling, as the thermospheric temperatures are much higher than those of L19 and those predicted by the model of Snowden & Yelle (2014) for similar HCN VMRs. The large change in HCN abundance from 2012 to 2014 ($L_S \sim 34°$–$56°$) and the seeming imbalance between its predicted cooling on the thermosphere may be the result of the recent change in Titan's postequinox stratospheric circulation, disruption of polar vortices, or other energetic events during the northern spring period (Teanby et al. 2012; Vinatier et al. 2015; Teanby et al. 2017; Coustenis et al. 2018; Teanby et al. 2019; Coustenis et al. 2020; Sharkey et al. 2020; Vinatier et al. 2020; Sharkey et al. 2021).

While the changes between temperature profiles from ~400 to 600 km appear anticorrelated with changes in the HCN VMR profiles, implying some cooling at these altitudes due to increased HCN atmospheric content, this effect is less efficient at these altitudes according to the model of Yelle (1991) and not enough to explain the largest difference of ~15 K between the 2015 and 2017 profiles. At these altitudes, vibrational emission from C_2H_6 also becomes important, though the profiles retrieved in the lower mesosphere with Cassini/CIRS do not show significant dispersion at low latitudes during this time period (Mathé et al. 2020). Unfortunately, the balance between HCN, C_2H_2, CH_4, and C_2H_6 cooling in the lower mesosphere is difficult to quantify with observations by ALMA due to the lack of observable transitions for these species in the (sub)millimeter.

4.2.2. Detached Haze Layer

Images of Titan from the Voyager and Cassini missions revealed the presence of a vertically variable, detached haze layer (Rages & Pollack 1983; Porco et al. 2005; West et al. 2011, 2018; Seignovert et al. 2021) later linked to the top of Titan's stratospheric meridional circulation (Rannou et al. 2004; Lebonnois et al. 2012; Larson et al. 2015), as its seasonal evolution cannot be explained by microphysical processes alone (Cours et al. 2011). The efficient absorption of solar photons by the dense haze in Titan's lower mesosphere was also found to manifest as a sharp inversion in thermal profiles derived from ground-based and Cassini/UVIS stellar occultations, as well as in the Huygens/HASI data (Sicardy et al. 1999; Fulchignoni et al. 2005; Sicardy et al. 2006; Lavvas et al. 2009; Koskinen et al. 2011). High-cadence images near Titan's

2009 spring equinox by Cassini/ISS showed the altitude of the detached haze layer descending rapidly from ∼500 to ∼350 km between 2008 and 2011 along with the collapse of the main haze (West et al. 2011; Seignovert et al. 2017; West et al. 2018; Seignovert et al. 2021), resulting in similar postequinox altitudes to that observed by Voyager 2 after Titan's spring equinox in 1980 (357 km at the equator; Rages & Pollack 1983). The consistent haze altitudes between 300 and 500 km and their subsequent descent near equinox were corroborated by Cassini/UVIS and ground-based occultations during both the 1980 and 2009 spring equinoxes (Sicardy et al. 1999, 2006; Liang et al. 2007; Koskinen et al. 2011) and through general circulation models of Titan's atmosphere (Rannou et al. 2002; Lebonnois et al. 2012; Larson et al. 2015). However, the temporal and spatial nature of the occasionally multiple, transient detached haze layers and plumes indicates a complex relationship between dynamics and microphysics that has proven difficult to predict on short timescales through current modeling efforts.

In the ALMA temperature profiles presented here, we find similar inversions in the 2012, 2015, and 2017 ($L_S \sim 34°$, 68°, and 89°) observations to those derived from occultation observations (Figure 7 inset; Figure 9, bottom panel, blue lines). The local temperature maximum in 2012 at 350 km (2.6×10^{-2} mbar) is in agreement with the altitudes of the detached haze layer shortly after equinox, as observed by Cassini and Voyager 2 (Rages & Pollack 1983; West et al. 2011), following the disruption of Titan's pole-to-pole circulation cell and the descent of the haze layer. Contemporaneous Cassini/ISS images indicate that this feature may be transient or a secondary descending layer that manifests during the disappearance of the main detached haze layer below 300 km (Seignovert et al. 2021). Similarly, the inversion found in 2015 ($L_S \sim 68°$) at 420 km (6.8×10^{-3} mbar) does not appear to correspond to a stable, postequinox haze layer through comparison with Cassini/ISS extinction profiles, though the 2017 ($L_S \sim 89°$) feature at similar altitudes aligns with the stable layer observed close to the end of the Cassini mission (West et al. 2018; Seignovert et al. 2021).

The absence of this feature in 2014 ($L_S \sim 56°$) and its subsequent reemergence in 2015 and 2017 ($L_S \sim 68°$ and 89°) is in agreement with dynamical models of Titan's atmosphere, marking the seasonal separation of haze due to Titan's strengthening meridional circulation approaching solstice (Lebonnois et al. 2012; Larson et al. 2015). These altitudes are similar to those found in the temperature inversions observed by Sicardy et al. (1999) in 1989, nearly one full Titan year prior. However, as the morphology of the haze layer appears inhomogeneous with latitude and longitude (West et al. 2011; Seignovert et al. 2021), the nature of the detached haze layer is difficult to quantify through the temperature inversions discussed here due to the relatively large ALMA beam footprint on Titan's disk. The ALMA resolution also smooths out small, latitudinally dependent vertical temperature perturbations, which complicates interpretations of these features and direct comparisons with previous observations. Further, while the measurement of temperature inversions was consistent across multiple retrievals (Figure 3), the magnitudes of these deviations are close to the corresponding retrieval errors (Figure 7). As such, it must be cautioned that the relation of these temperature features to the location of the detached or transient haze layer is tenuous and somewhat dependent on the confirmation of the latter from contemporaneous observations (e.g., those from Cassini/ISS or occultation measurements). Future ALMA observations at higher spatial resolution may present the opportunity to confirm this tentative connection and analyze the migration of the haze layer in a more meaningful way than presented here. Those observations would enable more comprehensive studies of the temporal and latitudinal evolution of Titan's haze after the end of the Cassini mission.

4.3. Considerations and Future Work

As the relative spatial and temporal scales enabled by the archival ALMA observations do not allow for the full analysis of temperature and HCN variability over relevant scales for Titan's upper atmosphere (e.g., a few Earth days, across latitude and local time), a number of considerations must be accounted for that constrain the interpretation of the results presented here. First, we note that a direct comparison between our ALMA results and those derived from HASI, INMS, and spacecraft occultation measurements is difficult due to the limitations of vertical and spatial resolution imposed by ground-based remote sensing measurements. As a result, these observations are not sensitive to vertical structure variability (e.g., those seen by Fulchignoni et al. 2005; Müller-Wodarg et al. 2006; Snowden et al. 2013) due to wave activity, which may account for additional temperature variability at these altitudes on the order 10 K (Strobel 2006). Similarly, the necessity to simultaneously retrieve the vertical temperature and HCN profiles from nadir and limb geometries somewhat obfuscates the direct assessment of Titan's atmospheric state at individual locations, as longitudinal and diurnal effects in HCN abundance and temperature may be introduced into the retrieved profiles (de La Haye et al. 2008; Cui et al. 2016).

As addressed in previous studies, complex atmospheric changes with latitude on Titan are not well resolved due to the relatively large ALMA beam size (Thelen et al. 2018, 2019b). This effect results in smoothing of vertical profiles over large latitude regions. While previous analyses with Cassini have shown no correlation between neutral thermospheric temperatures and latitude or longitude (Snowden et al. 2013), a full latitudinal map of mesospheric temperature profiles would considerably facilitate comparisons with models of Titan's atmosphere. Though beyond the scope of this work, additional latitude points may be analyzed from 2016 and 2017 observations to characterize the variability of upper atmosphere temperatures with latitude. Higher angular resolution observations will also enable an improved assessment of the effects of wind shear and dynamics on these temperature profiles. Higher-cadence observations would allow for the measurement of temperature variability in Titan's mesosphere to quantify diurnal effects and those of Saturn's magnetosphere, providing a comparison to measurements by Cassini/INMS in Titan's thermosphere (Snowden et al. 2013; Cui et al. 2016). A study of the monthly evolution of the mesospheric temperatures and winds during mid-2014 may be possible using additional ALMA archive observations. Finally, future observations with ALMA may assist with the development of updated spacecraft engineering models (e.g., for NASA's future Dragonfly mission), such as that of Yelle et al. (1997) for the Huygens probe.

5. Conclusions

Through the analysis of yearly ALMA observations of Titan from 2012 to 2017 ($L_S \sim 34°$–$89°$), we found large variability in the temperature and HCN abundance of Titan's mesosphere and thermosphere. The largest variation in mesospheric temperatures occurs between 2014 and 2015 ($L_S \sim 56°$ and 68°), where the mesopause shifts dramatically upward by 250 km from 563 ± 10 to 812 ± 42 km and cools from 153.7 ± 4.0 to 134.9 ± 3.4 K (Figure 9). The observed mesopause at both ~600 and ~800 km during this epoch agrees with prior observations by Cassini and Keck II and corroborates the results of models of Titan's atmosphere; however, the large variability observed here provides further challenges for modeling Titan's thermal structure in the mesosphere and stratosphere. Smaller temperature changes in the thermosphere and lower mesosphere may be explained by previously observed perturbations in exogenic energy sources, such as charged particle precipitation and interactions with Saturn's magnetosphere, which occur on timescales shorter than the observations analyzed here. Though latitudinal gradients in temperature were not derived from these observations, dynamical instabilities related to Titan's thermospheric jet (L19; Cordiner et al. 2020) may account for differences in the 2016 and 2017 ($L_S \sim 82°$ and 89°) profiles. In the lower mesosphere, we retrieve small inversions in the 2012, 2015, and 2017 temperature profiles that may be indicative of the location of transient or detached haze layers located between ~350 and 420 km following Titan's spring equinox, similar to prior observations during this time period by Cassini and 1 Titan yr before by Voyager 2 and ground-based observations.

Similarly large variability is found in Titan's HCN abundance, which extends the observed thermospheric HCN by an order of magnitude, with measurements from ALMA and Cassini now comprising VMRs from $\sim 3 \times 10^{-5}$ to 3×10^{-3} above 900 km. While the range in HCN abundance from year to year may account for deviations in the temperature profile from 2012—which is relatively warm, while the HCN abundance is fairly low—and minor temperature differences in the lower mesosphere and thermosphere, the temperatures retrieved for 2014, 2015, and 2017 require energy sources in addition to HCN cooling, solar UV/EUV heating, and wind shear. These sources may include variability in the abundances of Titan's other atmospheric species produced through photochemistry, such as C_2H_2 or C_2H_6, wave activity, or energy transfer from Titan's lower atmosphere during the seasonal transition to northern summer.

Future observations with ALMA may help to further elucidate the connection between Titan's upper atmospheric temperature and HCN abundance through dedicated, high-resolution observations over short timescales (i.e., <10 Earth days), where diurnal differences and those due to Titan's orbital position relative to the Saturnian plasma environment are relevant. While the variability of Titan's thermosphere was explored during the Cassini era, mesospheric temperature differences with latitude, longitude, and local time may be assessed through the unique capabilities of ground-based (sub)millimeter facilities such as ALMA. In particular, these observations are pertinent in the period around Titan's upcoming autumnal equinox in 2025, where similarly large variations in mesospheric temperature may manifest.

The authors wish to acknowledge the insightful discussion and comments from E. Lellouch regarding ALMA data analysis and radiative transfer modeling and the helpful suggestions from two anonymous reviewers that improved the quality of the final manuscript.

A.E.T. was funded by an appointment to the NASA Astrobiology Postdoctoral Program at Goddard Space Flight Center, administered by the USRA and ORAU through a contract with NASA. C.A.N. and M.A.C. were supported for their contributions to this work by NASA's Solar System Observations (SSO) Program. N.A.T. was funded by the UK Science and Technology Facilities Council.

This paper makes use of the following ALMA data: ADS/JAO.ALMA#2012.0.00727.S, 2 012.1.00635.S, 2 013.1.00446.S, 2 015.1.01023.S, and 2016.A.00014.S. ALMA is a partnership of ESO (representing its member states), NSF (USA) and NINS (Japan), together with NRC (Canada), MOST and ASIAA (Taiwan), and KASI (Republic of Korea), in cooperation with the Republic of Chile. The Joint ALMA Observatory is operated by ESO, AUI/NRAO and NAOJ. The National Radio Astronomy Observatory is a facility of the National Science Foundation operated under cooperative agreement by Associated Universities, Inc.

Some of the figures within this paper were produced using IDL color blind–friendly color tables (see Wright 2017).

ORCID iDs

Alexander E. Thelen https://orcid.org/0000-0002-8178-1042
Conor A. Nixon https://orcid.org/0000-0001-9540-9121
Martin A. Cordiner https://orcid.org/0000-0001-8233-2436
Nicholas A. Teanby https://orcid.org/0000-0003-3108-5775
Claire E. Newman https://orcid.org/0000-0001-9990-8817
Patrick G. J. Irwin https://orcid.org/0000-0002-6772-384X
Steven B. Charnley https://orcid.org/0000-0001-6752-5109

References

Aboudan, A., Colombatti, G., Ferri, F., & Angrilli, F. 2008, P&SS, 56, 573
Adriani, A., Dinelli, B. M., López-Puertas, M., et al. 2011, Icar, 214, 584
Bell, J. M., Bougher, S. W., Waite, J. H., et al. 2010, JGRE, 115, E12002
Bell, J. M., Hunter Waite, J., Westlake, J. H., et al. 2014, JGRA, 119, 4957
Bell, J. M., Westlake, J., & Waite, J. H. J. 2011, GRL, 38, L06202
Bertucci, C., Hamilton, D. C., Kurth, W. S., et al. 2015, GRL, 42, 193
Briggs, D. S. 1995, PhD thesis, New Mexico Inst. of Mining and Technology
Cordiner, M. A., Garcia-Berrios, E., Cosentino, R. G., et al. 2020, ApJL, 904, L12
Cours, T., Burgalat, J., Rannou, P., et al. 2011, ApJL, 741, L32
Courtin, R., Swinyard, B. M., Moreno, R., et al. 2011, A&A, 536, L2
Coustenis, A., Jennings, D. E., Achterberg, R. K., et al. 2018, ApJL, 854, L30
Coustenis, A., Jennings, D. E., Achterberg, R. K., et al. 2020, Icar, 344, 113413
Creecy, E. C., Li, L., Jiang, X., et al. 2019, GeoRL, 46, 13,649
Creecy, E. C., Li, L., Jiang, X., et al. 2021, GeoRL, 48, e95356
Cui, J., Cao, Y. T., Lavvas, P. P., & Koskinen, T. T. 2016, ApJL, 826, L5
Cui, J., Yelle, R. V., Vuitton, V., et al. 2009, Icar, 200, 581
de La Haye, V., Waite, J. H., Cravens, T. E., et al. 2008, JGRA, 113, A11314
Dobrijevic, M., Loison, J. C., Hue, V., & Cavalié, T. 2021, Icar, 364, 114477
Flasar, F. M., Achterberg, R. K., Conrath, B. J., et al. 2005, Sci, 308, 975
Flasar, F. M., Achterberg, R. K., & Schinder, P. J. 2014, Thermal Structure of Titan's Troposphere and Middle Atmosphere (Cambridge: Cambridge Univ. Press), 102
Flasar, F. M., Samuelson, R. E., & Conrath, B. J. 1981, Natur, 292, 293
Fomalont, E., van Kempen, T., Kneissl, R., et al. 2014, Msngr, 155, 19
Fulchignoni, M., Ferri, F., Angrilli, F., et al. 2005, Natur, 438, 785
Geballe, T. R., Kim, S. J., Noll, K. S., & Griffith, C. A. 2003, ApJL, 583, L39
Gordon, I. E., Rothman, L. S., Hargreaves, R. J., et al. 2022, JQSRT, 277, 107949
Gurwell, M. 2004, ApJ, 616, L7
Hanel, R., Conrath, B., Flasar, F. M., et al. 1981, Sci, 212, 192

Hidayat, T., Marten, A., Bézard, B., et al. 1997, Icar, 126, 170

Högbom, J. A. 1974, A&AS, 15, 417

Hörst, S. M. 2017, JGRE, 122, 432

Irwin, P. G. J., Teanby, N. A., de Kok, R., et al. 2008, JQSRT, 109, 1136

Jaeger, S. 2008, in ASP Conf. Ser. 394, Astronomical Data Analysis Software and Systems XVII, ed. R. W. Argyle, P. S. Bunclark, & J. R. Lewis (San Francisco, CA: ASP), 623

Kim, S. J., Geballe, T. R., & Noll, K. S. 2000, Icar, 147, 588

Kim, S. J., Geballe, T. R., Noll, K. S., & Courtin, R. 2005, Icar, 173, 522

Koskinen, T. T., Yelle, R. V., Snowden, D. S., et al. 2011, Icar, 216, 507

Larson, E. J. L., Toon, O. B., West, R. A., & Friedson, A. J. 2015, Icar, 254, 122

Lavvas, P., Yelle, R. V., & Vuitton, V. 2009, Icar, 201, 626

Lebonnois, S., Burgalat, J., Rannou, P., & Charnay, B. 2012, Icar, 218, 707

Lellouch, E., Gurwell, M. A., Moreno, R., et al. 2019, NatAs, 3, 614

Lellouch, E., Hunten, D. M., Kockarts, G., & Coustenis, A. 1990, Icar, 83, 308

Li, L. 2015, NatSR, 5, 8239

Liang, M.-C., Yung, Y. L., & Shemansky, D. E. 2007, ApJL, 661, L199

Lindal, G. F., Wood, G. E., Hotz, H. B., et al. 1983, Icar, 53, 348

Loison, J. C., Hébrard, E., Dobrijevic, M., et al. 2015, Icar, 247, 218

Lorenz, R. D., Young, L. A., & Ferri, F. 2014, Icar, 227, 49

Magee, B. A., Waite, J. H., Mandt, K. E., et al. 2009, P&SS, 57, 1895

Marten, A., Hidayat, T., Biraud, Y., & Moreno, R. 2002, Icar, 158, 532

Mathé, C., Vinatier, S., Bézard, B., et al. 2020, Icar, 344, 113547

Molter, E. M., Nixon, C. A., Cordiner, M. A., et al. 2016, AJ, 152, 42

Moreno, R., Marten, A., & Hidayat, T. 2005, A&A, 437, 319

Müller, H. S. P., Thorwirth, S., Roth, D. A., & Winnewisser, G. 2001, A&A, 370, L49

Müller-Wodarg, I. C. F., Yelle, R. V., Borggren, N., & Waite, J. H. 2006, JGRA, 111, A12315

Müller-Wodarg, I. C. F., Yelle, R. V., Cui, J., & Waite, J. H. 2008, JGRE, 113, E10005

Müller-Wodarg, I. C. F., Yelle, R. V., Mendillo, M., Young, L. A., & Aylward, A. D. 2000, JGR, 105, 20833

Paubert, G., Marten, A., Rosolen, C., Gautier, D., & Courtin, R. 1987, BAAS, 19, 633

Porco, C. C., Baker, E., Barbara, J., et al. 2005, Natur, 434, 159

Rages, K., & Pollack, J. B. 1983, Icar, 55, 50

Rannou, P., Hourdin, F., & McKay, C. P. 2002, Natur, 418, 853

Rannou, P., Hourdin, F., McKay, C. P., & Luz, D. 2004, Icar, 170, 443

Rengel, M., Shulyak, D., Hartogh, P., et al. 2022, A&A, 658, A88

Rymer, A. M., Smith, H. T., Wellbrock, A., Coates, A. J., & Young, D. T. 2009, GRL, 36, L15109

Schinder, P. J., Flasar, F. M., Marouf, E. A., et al. 2012, Icar, 221, 1020

Schinder, P. J., Flasar, F. M., Marouf, E. A., et al. 2020, Icar, 345, 113720

Seignovert, B., Rannou, P., Lavvas, P., Cours, T., & West, R. A. 2017, Icar, 292, 13

Seignovert, B., Rannou, P., West, R. A., & Vinatier, S. 2021, ApJ, 907, 36

Serigano, J., Nixon, C. A., Cordiner, M. A., et al. 2016, ApJ, 821, L8

Sharkey, J., Teanby, N. A., Sylvestre, M., et al. 2020, Icar, 337, 113441

Sharkey, J., Teanby, N. A., Sylvestre, M., et al. 2021, Icar, 354, 114030

Shemansky, D. E., Stewart, A. I. F., West, R. A., et al. 2005, Sci, 308, 978

Sicardy, B., Colas, F., Widemann, T., et al. 2006, JGRE, 111, E11S91

Sicardy, B., Ferri, F., Roques, F., et al. 1999, Icar, 142, 357

Smith, G. R., Strobel, D. F., Broadfoot, A. L., et al. 1982, JGR, 87, 1351

Snowden, D., & Higgins, A. 2021, Icar, 354, 113929

Snowden, D., & Yelle, R. V. 2014, Icar, 228, 64

Snowden, D., Yelle, R. V., Cui, J., et al. 2013, Icar, 226, 552

Strobel, D. F. 2006, Icar, 182, 251

Sylvestre, M., Teanby, N. A., Vatant d'Ollone, J., et al. 2020, Icar, 344, 113188

Teanby, N. A., Bézard, B., Vinatier, S., et al. 2017, NatCo, 8, 1586

Teanby, N. A., de Kok, R., Irwin, P. G. J., et al. 2008, JGRE, 113, E12003

Teanby, N. A., Irwin, P. G. J., de Kok, R., et al. 2007, Icar, 186, 364

Teanby, N. A., Irwin, P. G. J., Nixon, C. A., et al. 2012, Natur, 491, 732

Teanby, N. A., Sylvestre, M., Sharkey, J., et al. 2019, GRL, 46, 3079

Thelen, A. E., Cordiner, M., Nixon, C. A., et al. 2019b, AGUFM, 2019, P21C

Thelen, A. E., & Molter, E. M. 2018, Spatially Resolved Spectrum Extraction Script, Mendeley Data, Version 1

Thelen, A. E., Nixon, C. A., Chanover, N. J., et al. 2018, Icar, 307, 380

Thelen, A. E., Nixon, C. A., Chanover, N. J., et al. 2019a, Icar, 319, 417

Vervack, R. J., Sandel, B. R., & Strobel, D. F. 2004, Icar, 170, 91

Vinatier, S., Bézard, B., Lebonnois, S., et al. 2015, Icar, 250, 95

Vinatier, S., Mathé, C., Bézard, B., et al. 2020, A&A, 641, A116

Vuitton, V., Yelle, R. V., Klippenstein, S. J., Hörst, S. M., & Lavvas, P. 2019, Icar, 324, 120

Vuitton, V., Yelle, R. V., & McEwan, M. J. 2007, Icar, 191, 722

West, R. A., Balloch, J., Dumont, P., et al. 2011, JGRL, 38, L06204

West, R. A., Seignovert, B., Rannou, P., et al. 2018, NatAs, 2, 495

Westlake, J. H., Bell, J. M., Waite, J. H. J., et al. 2011, JGRA, 116, A03318

Willacy, K., Allen, M., & Yung, Y. 2016, ApJ, 829, 79

Wright, P. 2017, ColourBlind: A Collection of Colour-blind-friendly Colour Tables, Zenodo, doi:10.5281/zenodo.840393

Yelle, R. V. 1991, ApJ, 383, 380

Yelle, R. V., Borggren, N., de la Haye, V., et al. 2006, Icar, 182, 567

Yelle, R. V., Cui, J., & Müller-Wodarg, I. C. F. 2008, JGRE, 113, E10003

Yelle, R. V., & Griffith, C. A. 2003, Icar, 166, 107

Yelle, R. V., Snowden, D. S., & Müller-Wodarg, I. C. F. 2014, Titan's Upper Atmosphere: Thermal Structure, Dynamics, and Energetics (Cambridge: Cambridge Univ. Press), 322

Yelle, R. V., Strobell, D. F., Lellouch, E., & Gautier, D. 1997, in ESA Special Publication, Vol. 1177, Huygens: Science, Payload and Mission, ed. A. Wilson, 243